TOPICAL REVIEW • OPEN ACCESS

Physical properties of bulk, defective, 2D and 0D metal halide perovskite semiconductors from a symmetry perspective

To cite this article: Claudio Quarti *et al* 2020 *J. Phys. Mater.* **3** 042001

View the article online for updates and enhancements.

Journal of Physics: Materials

TOPICAL REVIEW

Physical properties of bulk, defective, 2D and 0D metal halide perovskite semiconductors from a symmetry perspective

Claudio Quarti[1,2] (iD), **Claudine Katan**[1] **and Jacky Even**[3]

1 Univ Rennes, ENSCR, INSA Rennes, CNRS, ISCR (Institut des Sciences Chimiques de Rennes) - UMR 6226, F-35000 Rennes, France
2 Laboratory for Chemistry of Novel Materials, Department of Chemistry, Université de Mons, place du Parc 20, Mons 7000, Belgium
3 Univ Rennes, INSA Rennes, CNRS, Institut FOTON - UMR 6082, F-35000 Rennes, France

E-mail: claudio.quarti@univ-rennes1.fr

Abstract

Metal halide perovskite-based nanostructures, nanosheets and nanoparticles at the forefront, show attractive optoelectronic properties, suitable for photovoltaics and light emission applications. Achieving a sounded understanding of these basic electronic and optical properties represents therefore a crucial step for the full technological exploitation of this class of semiconductors. The rapidly expanding chemical engineering and their unusual structural diversity is fascinating but also challenging for a rational description on par with those well-known for conventional semiconductors. In this sense, group theory-based symmetry analyses offer a general and rigorous approach to understand the properties of various bulk perovskites and perovskite-based nanostructures. In this work, we review the electronic and optical response of metal halide perovskite semiconductors using symmetry analysis from group theory, recalling the main results for the prototypical cubic Pm-3m lattice of AMX_3 bulk perovskites (where A is cation, M metal and X halide), then extending the analysis to three cases of technological interest: AMX_3 nanoparticles, A_4MX_6 isolated octahedra, A_2MX_4 layered systems, and recently introduced deficient halide perovskites (d-HP). On the basis of symmetry arguments, we will stress analogies and differences in the electronic and optical properties of these materials, as induced by the spatial confinement and dimensionality. Meanwhile, we will take advantage of this analysis to discuss recent results and debates from the literature, as the energetics of dark/bright states in the band-edge exciton fine structure of perovskite nanoparticles and nanosheets. From the present work, we also anticipate that the band-edge exciton fine structure of d-HP does not present optically dark states, in striking contrast to AMX_3 nanoparticles and layered perovskites, a fact that can have important consequences on the photophysics of these novel perovskitoids.

1. Introduction

Metal halide perovskites have swiftly surged as promising semiconducting materials, during the last decade, thanks to their huge potential for optoelectronic applications. Since the pioneering demonstration in 2009 of their ability to convert light into current in dye sensitized solar cell architectures [1], and the decisive demonstration in 2012 of their inherent transport properties [2], halide perovskites have encountered an unprecedented success, most notably in photovoltaics and light emission. In photovoltaics, these materials have marked an impressive series of light-to-current efficiency records [3–8], with best performing perovskite-based single-junction and tandem cells showing certified 25.2% and 29.1% efficiency, respectively [9], and currently 16.1% for small modules [10]. Application of metal halide perovskites to light emission has also demonstrated comparable success, with reports of external quantum efficiencies overcoming 20% [11–14], challenging long-time established thin-film technologies. Halide perovskites present AMX_3 stoichiometry, with M corresponding to a divalent metal (Pb, Sn, Ge) and X to a halide, and their building

Figure 1. Graphical schematization of different perovskite-derivate structures discussed in this work. At the center, the building block of the perovskite structure is depicted, corresponding to the MX_6 octahedron and the A cation (as exemplified by methylammonium). The other investigated structures consist in: native 3D perovskite bulk structure and related dimensionally confined nanostructures, MX_6 isolated octahedra, layered 2D halide perovskites in the Dion–Jacobson (DJ) and Ruddlesden–Popper (RP) phases, hollow [21–23] and deficient halide perovskites (d-HP) [24, 25].

block is constituted by continuous network of MX_6 octahedra connected in corner-shared fashion (see figure 1). The A cation instead consists in a small organic molecule (methylammonium, or formamidinium) or an inorganic atom (Cs), which fills the cavities between the octahedral and guarantees the charge neutrality of the chemical unit. The astonishing performances of these materials are mainly related to their unique electronic structure that combines effective optical absorption [15], defect tolerance [16, 17], and reduced charge recombination [18], which in turn determine their long photo-carrier diffusion[19, 20] and effective light emission.

A peculiarity of these materials is their intrinsic chemical and structural tailorability, that is the possibility to widely tune their chemical composition. This allows to easily obtain complex nanostructures, ranging from bulk three-dimensional (3D) single crystals, layered two-dimensional (2D) nanosheets, down to 0D-like quantum dots, with size on the order of few tens of nanometers [26, 27], or few nanometers, ideally down to isolated MX_6 octahedra [28, 29]. Confinement of the charge carriers at the nanoscale imparts unique optoelectronic features to halide perovskites, with interesting implications for technologic applications. 0D halide perovskites nanoparticles revealed their high potential for various optoelectronic applications, including nowadays highest record efficiencies for quantum dot (16.6%) solar cells [30, 31]. In 2D layered halide perovskites, the semiconducting MX_6 corner-shared octahedral structure is sandwiched between two layers of (traditionally) insulating organic spacers [32, 33], with the consequent spatial and dielectric confinement imparting unique electronic and optical response to these systems [34]. The resulting sharp and effective excitonic emission is ideal for light emission application [35, 36]. In addition, the improved stability of 2D perovskites, compared to their 3D analogues, is currently exploited as possible strategy for long-time stable photovoltaic devices [7, 37]. The quest for new halide perovskite-derivatives and the exploration of low-dimension tailored nanostructures, also led recently to the design of the so called 'hollow' [21–23], and 'deficient' halide perovskite (d-HP) materials (see figure 1) [24, 25]. In these systems, the introduction of

large organic cations during the synthesis procedure results in the intentional formation of MX vacancies in the perovskite corner-shared pattern, but while for the case of 'hollow'-perovskites these defects are randomly distributed, for 'deficient'-perovskites they self-organize, as highlighted by the appearance at low angles of signals in the corresponding x-ray diffraction pattern. The local breaking of the MX_6 octahedral connectivity hardly affects the electronic properties and photovoltaic response of these materials, at least for low content of defects (~10%), but significantly improves the material stability compared to parental 3D systems, meanwhile reducing the content of toxic elements (Pb or Sn) lying at the M site [24, 25, 38].

The continuous exploration of the chemical space associated to metal halide perovskites calls for fundamental understanding of their physics and photophysics, inherently complicated by the interplay of many features like dynamic disorder [39–41], spin–orbit coupling (SOC) [42], many-body effects [43, 44], etc. Theoretical analysis of halide perovskites at the atomistic scale hence requires involved and computationally expensive methods, in order to properly describe the properties of these compounds, including many-body approaches, such as those based on the GW approximation [43, 44] and the solution of the Bethe–Salpeter Equations [45], molecular dynamic simulation techniques [39–41, 46, 47], methods including electron–phonon interactions, etc [48–50]. On the opposite side of the barricade, the use of simplified methods from the theory of conventional semiconductors, e.g. effective mass-based approaches [51, 52] or tight-binding models [53], have been successfully used in the past to describe the electronic and optical properties of halide perovskite structures. In particular, group theory-based symmetry analysis revealed a powerful tool to achieve a robust insight into the basic properties of these semiconductors [54–56]. With special focus on the optoelectronic properties of metal halide perovskites, in this work we show how symmetry analyses can anticipate important properties and support the interpretation of complex experiments, with references to the recent literature. Recalling the main results from group theory for the cubic α-phase of the $CH_3NH_3PbI_3$ halide perovskite [54, 55], taken as reference for 3D systems, we extend the symmetry analysis to the three cases of technological interest depicted in figure 1, namely perovskite nanoparticles, layered 2D halide perovskites and the d-HP introduced by Mercier and collaborators [24, 25].

The manuscript is organized as follows. We first discuss the electronic structure of these systems, in terms of hybridization of the orbitals of the composing atoms (linear combination of atomic orbitals (LCAO)) and in absence of SOC, in order to highlight the differences in the electronic structure induced by the dimensionality and spatial confinement. Then, we consider the effect of SOC, particularly important when heavy atoms (Sn, Pb) occupy the M site, and discuss the corresponding electronic structures and optical properties, from a symmetry viewpoint, with reference to recent results from the literature.

2. Dimensionality and confinement effects on the electronic structure of halide perovskites

The α-phase of metal halide perovskite systems belongs to the Pm-3m space group and is the reference structure for the 3D bulk perovskites. When considering the rotational disorder of the organic cation, the 'pseudo' version of this cubic phase is stable at room temperature for the prototypical hybrid $CH_3NH_3PbCl_3$ and $CH_3NH_3PbBr_3$ perovskites, while being accessible above 54 °C for $CH_3NH_3PbI_3$ [57], and at even higher temperatures for the all inorganic $CsPbI_3$ compound [58]. Thanks to its simplicity, this model structure represents the ideal case for a detailed symmetry analysis, meanwhile conveying important information on the properties of halide perovskites under realistic operative conditions. Single particle electronic wavefunctions of molecules and crystals can be conveniently expressed on the basis of the wavefunctions of the constituting atoms, in the formal frame of the LCAO [59]. Additionally, for crystalline solids, translational symmetry can be further exploited, which imposes the single particle states to have Bloch form [59, 60]:

$$\psi_{n,\mathbf{k}}(\mathbf{r}) = e^{i\mathbf{k}\mathbf{r}} u_{n,\mathbf{k}}(\mathbf{r}) \tag{1}$$

where $u_{n\mathbf{k}}(\mathbf{r})$ is a function with the same periodicity as the crystalline lattice, while $e^{i\mathbf{k}\mathbf{r}}$ accounts for the difference in the phase of the wavefunction in different cells. Because of the presence of the $\mathbf{k}$-vector in equation (1), one must consider the symmetry of the system both in the real and reciprocal space.

The strength of group theory analysis is that it determines which are the allowed combination of atomic orbitals in equation (1), without need to explicitly solve the Schrodinger equation. Furthermore, it provides a robust classification of the wavefunctions $\psi_{n,\mathbf{k}}(\mathbf{r})$ on the basis of irreducible representations (IR) of the space group of interest. This is practically done by evaluating the inner product $\chi_{site} \otimes \chi_{phys}$, involving the site-reducible representation (χ_{site}), associated to the symmetry and multiplicity of the specific atomic positions in the cell, and the IR associated to the physical observable of interest (χ_{phys}), in this case the symmetry of the atomic orbitals (s-, p-, etc.). Notably, χ_{site} contains also the information about the phase relation $e^{i\mathbf{k}\mathbf{r}}$ of equation (1).
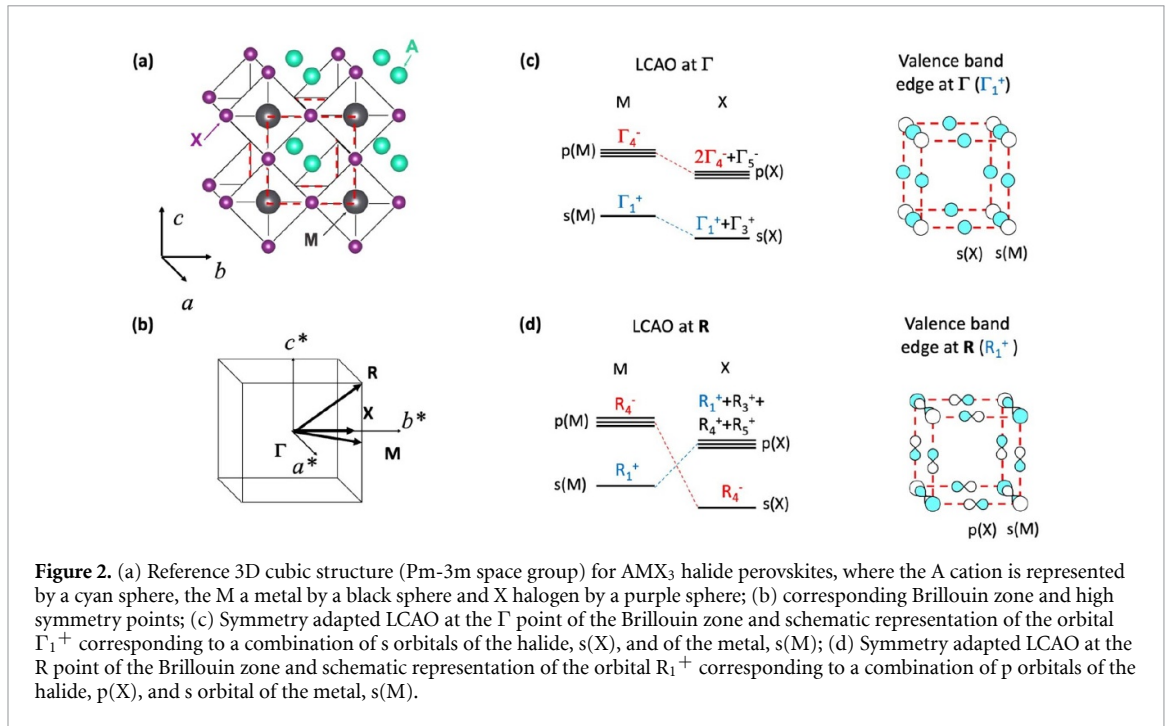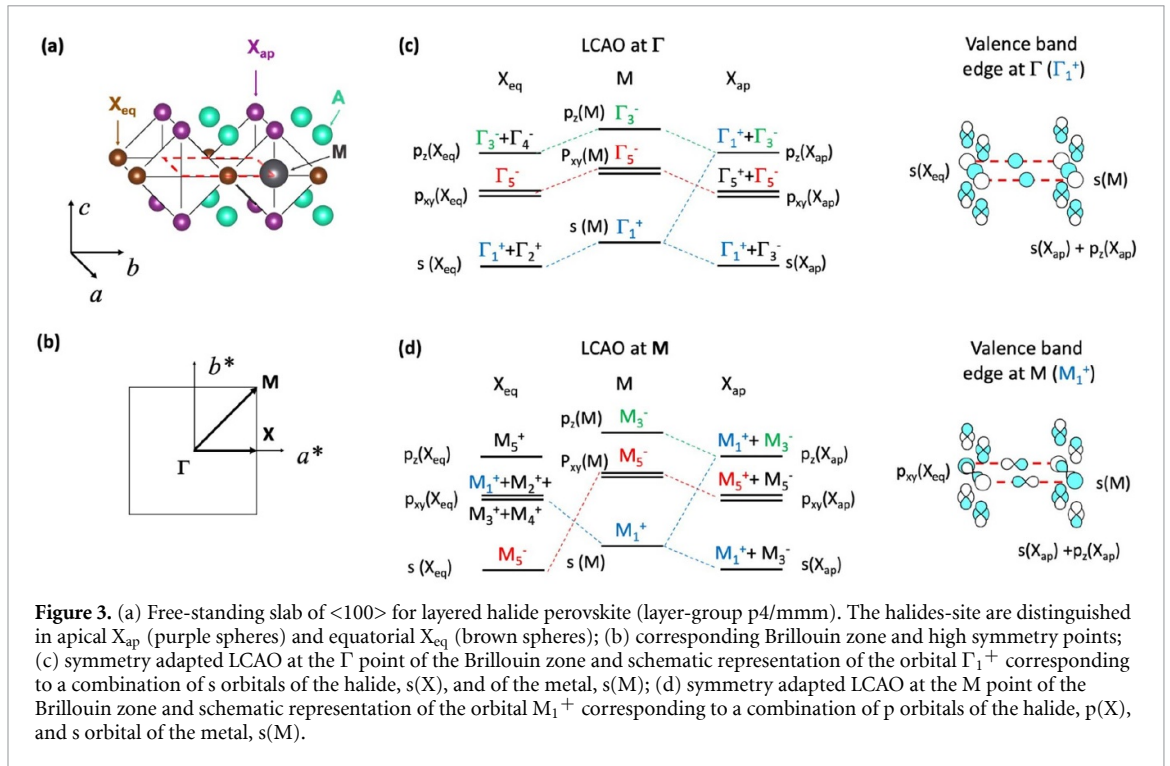
Figure 2. (a) Reference 3D cubic structure (Pm-3m space group) for AMX$_3$ halide perovskites, where the A cation is represented by a cyan sphere, the M a metal by a black sphere and X halogen by a purple sphere; (b) corresponding Brillouin zone and high symmetry points; (c) Symmetry adapted LCAO at the Γ point of the Brillouin zone and schematic representation of the orbital Γ_1^+ corresponding to a combination of s orbitals of the halide, s(X), and of the metal, s(M); (d) Symmetry adapted LCAO at the R point of the Brillouin zone and schematic representation of the orbital R_1^+ corresponding to a combination of p orbitals of the halide, p(X), and s orbital of the metal, s(M).

In the general case of both halide and oxide perovskites, the A cation is not involved in the formation of the frontier orbitals. For halide perovskites, we can hence conveniently express the LCAO expansion of the single particle electronic states on the minimal basis of the frontier s- and p- orbitals of the metal M and halide X, here-on named s(M), p(M), s(X), p(X). In our representation of figure 2(a) [54, 55], M lies in the Wyckoff position 'a' (0,0,0) and its site symmetry χ_{site} belongs to the total-symmetric IR, Γ_1^+ and R_1^+, at the points Γ and R of the corresponding Brillouin zone in figure 2(b). The character table of the Pm-3m space group is reported in the supporting information (available online at stacks.iop.org/JPMATER/03/042001/mmedia). The halide atoms lie in the Wyckoff position 'd' (1/2,0,0) and their reducible site symmetry χ_{site} belong to $\Gamma_1^+ + \Gamma_3^+$ and R_4^- IR, at the Γ and R points, respectively. The combination of these site symmetries with the IR of the s- (A_{1g}) and p- (T_{1u}) orbitals of the composing M and X atoms results in the LCAO hybridization in figures 2(c) and (d), highlighting strikingly different atomic combination at the Γ and R point of the Brillouin zone. In Γ, figure 2(c), the symmetry allowed atomic orbitals combinations are the s(M)–s(X) and p(M)–p(X) ones, corresponding to Γ_1^+ and Γ_4^- IR, while mixed s-p combinations are symmetry forbidden, as they belong to different IR. In R, figure 2(d), the s(M)–p(X) and p(M)–s(X) combinations are instead allowed and correspond to R_1^+ and R_4^- IR, respectively. Electronic structure calculations based on density functional theory (DFT) and many-body GW approximation performed on the α-phase of CsPbI$_3$ perovskites clearly showed direct band gap at the R point of the primitive cubic Brillouin zone [42, 44, 54, 61], with the valence and conduction band edges belonging to R_1^+ and R_4^- IR, respectively [54]. The smaller transition energy at R compared to Γ is easily explained in terms of the specific orbital hybridization highlighted in figures 2(c) and (d) [42, 61, 62]. In fact, the overlap between s(M)–p(X)/p(M)–s(X) atomic orbitals in figure 2(d) is expected to be larger than the overlap between s(M)–s(X) and the p(M)–p(X) in figure 2(c), because of the different spatial extension of the involved atomic orbitals. As result, the destabilization (stabilization) associated to the valence (conduction) band is expected to be larger in R than in Γ. Furthermore, symmetry anticipates that, in absence of SOC, the conduction band edge of metal halide systems is triply degenerate, being associated to a three-dimensional IR. This prediction should be reasonably accurate for AMX$_3$ perovskites containing light elements, while being definitely inaccurate in presence of tin and lead [42]. For the sake of example, for Germanium-based CH$_3$NH$_3$GeCl$_3$ perovskite, spin–orbit effects on the order of 0.15 eV were predicted from DFT [62].

Layered halide perovskites can be obtained by cutting the 3D bulk structure along specific crystallographic directions, with <100> family in figure 3(a) representing the most widely studied class of layered halide perovskites. Symmetry analysis of a free-standing monolayer 2D A$_2$MX$_4$ model system in figure 3(a) can be conveniently carried out using *layer-group* symmetry as a first step, that is, considering only one isolated periodic plane and neglecting plane stacking. <100> layered perovskites belong to tetragonal p4/mmm layer-group, with an electronic band gap at M in the corresponding first Brillouin zone, reported in figure 3(b). Before to evaluate the product $\chi_{site} \otimes \chi_{phys}$, for the present case, it is worth

Figure 3. (a) Free-standing slab of <100> for layered halide perovskite (layer-group p4/mmm). The halides-site are distinguished in apical X_{ap} (purple spheres) and equatorial X_{eq} (brown spheres); (b) corresponding Brillouin zone and high symmetry points; (c) symmetry adapted LCAO at the Γ point of the Brillouin zone and schematic representation of the orbital Γ_1^+ corresponding to a combination of s orbitals of the halide, s(X), and of the metal, s(M); (d) symmetry adapted LCAO at the M point of the Brillouin zone and schematic representation of the orbital M_1^+ corresponding to a combination of p orbitals of the halide, p(X), and s orbital of the metal, s(M).

mentioning that a symmetry reduction from cubic to tetragonal, is often observed for 3D perovskites as a result of a low temperature structural phase transition [57]. This reduction splits the triplet of halide atoms in the AMX_3 motif into an atom occupying a Wyckoff position along the tetragonal axis and a doublet of in-plane atoms. In the A_2MX_4 2D reference layer the quadruplet of halogen atoms yields a doublet of apical atoms and a doublet of equatorial atoms, figure 3(a), resulting in different site symmetries, χ_{site}. As shown in figures 3(c) and (d), p_{xy} and p_z orbitals are split, as they belong to E_u and A_{2u} IR, respectively, with consequently different definition of χ_{phys}. The character tables for single and double groups of the p4/mmm layer-group at the Γ and M points are related to the ones of the P4/mmm space group reported in the supporting information. The metal cation site symmetries for p4/mmm layer-group correspond to Γ_1^+ and M_1^+, at the Γ and M point of the 2D first Brillouin zone, reported in figure 3(b). The equatorial halides (X_{eq}) lie at Wyckoff positions 'c' and their site symmetries correspond to $\Gamma_1^+ + \Gamma_2^+$ and M_5^-. For the apical halide (X_{ap}), lying at the 'd' Wyckoff position, the site symmetry IR correspond to $\Gamma_1^+ + \Gamma_3^-$ and $M_1^+ + M_3^-$. The LCAO scheme of an isolated perovskite layer, as computed from the $\chi_{site} \otimes \chi_{phys}$ inner product at the Γ, figures 3(c), and (M) points of the Brillouin zone, figure 3(d), nicely parallels the hybridization found for the 3D case. At the Γ point, symmetry allowed combinations involve mixing between s(M)–s(X) and p(M)–p(X) orbitals, having Γ_1^+ and Γ_5^- IR, respectively. At M, instead, these combinations are not allowed anymore, while s(M)–p(X) and p(M)–s(X) combinations are permitted, corresponding to M_1^+ and M_5^- IR. Most notably, the electronic structure of layered perovskites shows an important difference, compared to the 3D case, namely that the original triply degenerate p(M)–s(X) combination found in the 3D system, figure 2(d), splits in a doubly degenerate state belonging to Γ_5^- and M_5^- IR and a non-degenerate state belonging to Γ_3^- and M_3^- IR, at the Γ and M point of the first Brillouin zone, respectively. This means that in layered systems, the p_{xy}(M)–s(X) hybridization inside the layer and p_z(M)–s(X) along orthogonal direction are decoupled, as they belong to two different IR, a fact that becomes important when the anisotropy of the optical properties is considered [63].

Although very weak inter-planar electronic coupling is expected, as due to the large spatial separation between planes, usually exceeding the radius of the s,p(M) s,p(X) atomic orbitals, vertical coupling may be further analyzed using 3D periodic space groups. In this frame, different patterns in the inter-plane packing can be relevant in terms of symmetry analysis. In fact, according to the nomenclature of oxide perovskites, the 2D layered systems can be classified in Dion–Jacobson (DJ), Ruddlesden–Popper (RP), in relation to the presence of one or two interlayer cations per formula unit, as shown in figure 1 [64]. Additionally, Aurivilius phase can also be found in presence of covalent network between the two-dimensional oxide perovskite slabs, but this case has not been observed in halide perovskites up to now. For halide perovskites, DJ and RP terms are conventionally used in the literature to define different inter-planar stacking, with DJ indicating a displacement of two consecutive perovskite planes close to an in-plane (0,0) translation and RP indicating a
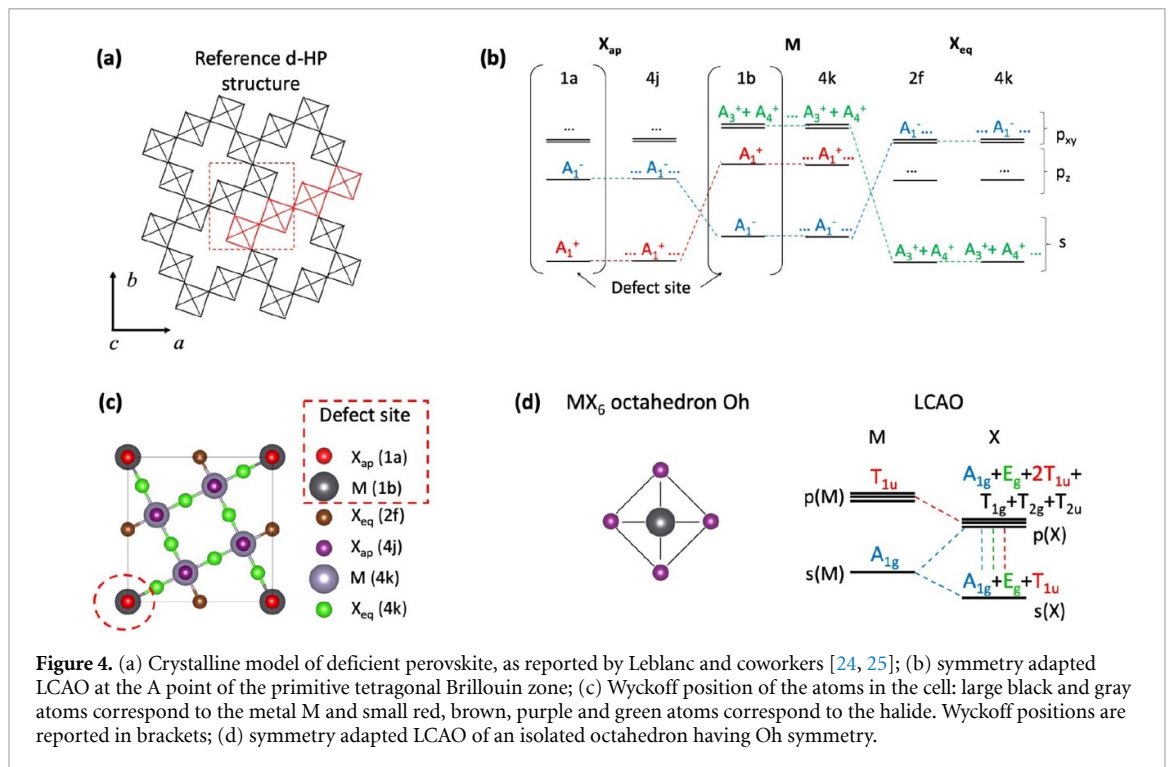
Figure 4. (a) Crystalline model of deficient perovskite, as reported by Leblanc and coworkers [24, 25]; (b) symmetry adapted LCAO at the A point of the primitive tetragonal Brillouin zone; (c) Wyckoff position of the atoms in the cell: large black and gray atoms correspond to the metal M and small red, brown, purple and green atoms correspond to the halide. Wyckoff positions are reported in brackets; (d) symmetry adapted LCAO of an isolated octahedron having Oh symmetry.

displacement close to a (1/2,1/2) translation. Within a tetragonal frame, we may define reference A_2MX_4 DJ and RP phases belonging to P4/mmm and I4/mmm space groups, respectively. Interestingly, we notice that these bulk layered crystallographic structures are formed by periodically repeating the <100> free-standing slab along the stacking axis. Therefore, the symmetry properties of these DJ and RP reference phases can be understood by mapping their 3D Brillouin zone onto the 2D Brillouin zone of the related p4/mmm layer space group. The case of the Cs_2PbI_4 reference RP phase is treated in the following from that perspective (vide infra).

Finally, we discuss the case of 'defective' halide perovskites, in terms both of its possible exploitation for photovoltaics, as related to its improved stability compared to 3D lead-halide perovskites, and as reference model to discuss the perturbation of the electronic structure of halide perovskites, as due to point defects (e.g. the MX vacancy). Dealing with this second aspect, it is worth to mention that the d-HP structure by Mercier *et al* is most likely not the most representative test-case for defects but it has the advantage to be realistic and is simple enough to allow a symmetry-based analysis. In particular, we will see how the introduction of a point defect results in the relaxation of the spectroscopic selection rules. As anticipated, Leblanc *et al* synthetized and characterized samples of deficient $CH_3NH_3PbI_3$ and $HC(NH_2)_2PbI_3$ perovskites, reporting XRD patterns consistent with a self-organization of the defects. From their diffraction measurements, these authors proposed the crystalline model reported in figure 4(a), belonging to the tetragonal P4/m space group and having cell 5 times larger than for parental pristine Pm-3m space group α-$CH_3NH_3PbI_3$ and α-$HC(NH_2)_2PbI_3$ [24, 25]. MX vacancies self-organize along channels parallel to the *c*-axis, with ideally empty channels in correspondence of one depleted metal cation each five chemical units. For this system, symmetry analysis should be carried out at the A point of the first Brillouin zone of the primitive tetragonal lattice [25], as this corresponds to the R point of the parental Pm-3m space group (see supporting information). The complete evaluation of the product $\chi_{site} \otimes \chi_{phys}$ for this system reveals quite complicated, because of the presence of the same chemical species in different Wyckoff positions, as classified in figure 4(b, c), and because the symmetry reduction relaxes the constraints, allowing many more possible atomic orbitals hybridizations, compared to the Pm-3m lattice. The resulting symmetry adapted LCAO at the A point of the Brillouin zone is summarized in figure 4(c), with the full scheme reported in the supporting information. Most notably, in figure 4(c) we can find again similar interactions as in the cubic Pm-3m lattice. For the valence band, the hybridization of $p(X_{eq/ap})$–$s(M)$ is still allowed for A_1^- IR, with the X_{eq} and X_{ap} halides responsible for the hybridization within the tetragonal plane and along the *c*-axis, respectively. For the conduction band, the symmetry reduction brings to a splitting of the original triply degenerate $s(X)$–$p(M)$ combination into a two-fold $p_{xy}(X)$–$s(M)$ combination with $A_3^+ + A_4^+$ symmetry and non-degenerate $p_z(X)$–$s(M)$ combination of A_1^+ symmetry. On the basis of this LCAO scheme, the effect of MX vacancy channels along *c*-axis can be easily anticipated, as this interrupts the MX bonding alternation in

the *ab*-plane after four MX_6 octahedra, as highlighted in figure 4(a), while preserving continuous MX channels along the *c*-direction. As a result, the valence band is expected to be less sensitive to the introduction of MX vacancies, as it is characterized by electronic dispersion both within the tetragonal plane and along the orthogonal *c*-axis. Similarly, the conduction state with A_1^+ symmetry, involving $s(X_{ap})$–$p_z(M)$ hybridization along *c*, preserves in large part its electronic communication, while the $A_3^+ + A_4^+$ conduction state, involving in-plane $s(X_{eq})$–$p_{xy}(M)$ hybridization will be significantly destabilized by the defect channels, as discussed in [25]. Summarizing, introduction of MX vacancy in d-HP results in a splitting of the triply degenerate p(M)-s(X) conduction states into doubly degenerate in-plane and non-degenerate out-of-plane components, as for the reference 2D case, in figure 3(d). However, while in the latter, the electrons are fully delocalized in the tetragonal *ab*-plane, in the case of d-HP, they preserve the full electronic conjugation along the *c*-axis, hence likely presenting more one dimensional-like electronic and optical properties.

At the bottom step of the ladder for spatially confined perovskite-derivate structures, we obviously find the isolated MX_6 octahedron, corresponding to the case where the octahedral connectivity is interrupted along all directions. The symmetry of this system can be analyzed as well [55], taking advantage of the lacking of translational symmetry and adopting point group symmetry, corresponding to Oh, for an ideal geometry with equal MX bond lengths and all angles of 90 and 180 degrees. The determination of the product $\chi_{site} \otimes \chi_{phys}$ is routinely performed, with the only difference with respect to the previous 3D, 2D and d-HP cases that no phase factors as in equation (1) should be considered. The reducible site symmetry of the halides is clearly six-dimensional, corresponding to $A_{1g} + E_g + T_{1u}$. The corresponding hybridization scheme for the isolated MX_6 octahedron is reported in figure 4(d), globally showing more symmetry allowed LCAO combinations, compared to the simple 3D and 2D case. For instance, while the mixing of s(M) and p(M) states is still forbidden, as in the case of both the 3D and 2D structures, mixing between both s(X) and p(X) is allowed for the isolated octahedron, under three different IR (A_{1g}, E_g, T_{1u}). Similarly, while the combinations between s(M)–s(X) and s(M)–p(X) states are forbidden in the 3D Pm-3m case for the same point of the Brillouin zone (see figures 2(c) and (d)), these are allowed for the isolated octahedron. Altogether, the lack of translational symmetry in the case of one MX_6 octahedron and presence of more halides per chemical units compared to the 3D and 2D cases results in more complex electronic hybridization scheme. Most noteworthy, the electronic structure of the MX_6 octahedron still allows for the s(M)–p(X) and p(M)–s(X) with A_{1g} and T_{1u} symmetry respectively, which in the 3D case correspond to the frontier orbitals [54]. One should however take care in assigning the frontier highest-occupied molecular orbital and lowest unoccupied molecular orbitals levels of the isolated MX_6 octahedron to A_{1g} and T_{1u} symmetry, as this is not general. Maughan *et al* in fact proposed different assignments for isolated SnI_6 octahedra [65], as well as in solid state, for the case of vacancy order cesium tin-iodide perovskite [65, 66]. As the present paper mainly focuses on lead-based systems, we will discuss later the specific case of Cs_4PbBr_6, a system with crystalline structure consisting in isolated $PbBr_6$ octahedra, spaced by Cs cations, showing striking efficient photoluminescence quantum efficiencies (PLQY ~45%) [67, 68].

Before to conclude, we briefly comment on the symmetry analysis of AMX_3 nanoparticles, representing a special case, where the octahedral connectivity is still present, although limited to ~tens of chemical units in length, and where the size and shape of the nanoparticle itself can influence the optical and electronic properties of the system. In this sense, the electronic density of states of perovskite quantum nanostructures also exhibit delta-like features but the optoelectronic properties of these 0D nano-objects are strongly dependent on the symmetry properties of the parental perovskite lattice. Due the large number of atoms (typically about 50 000 atoms for a cubic $CsPbBr_3$ quantum dot with a lateral size of 12 nm), the description of the electronic structure shall rely on empirical methods. One of the advantages of a fully atomistic supercell tight-binding model is that it does not require any approximation on the QD shape, leading to simulations using very realistic geometries and scaling up to a few millions atoms [69]. However, the available symmetry-based perovskite tight-binding model [53] has not yet being extended from the 3D lattice to a 0D perovskite nanostructure. The most common description for semiconductor nanostructure relies on a k.p multiband effective mass approximation for the description of the bulk electronic structure and envelope functions allowing to account for the size and shape of the nanostructure:

$$\psi_i(\mathbf{r}) = \sum_n f_{i,n}(\mathbf{r}) u_{n,\mathbf{k}_0}(\mathbf{r}) \tag{2}$$

where $\psi_i(\mathbf{r})$ is a monoelectronic wavefunction of the nanostructure, $u_{n,\mathbf{k}_0}(\mathbf{r})$ are the bulk Bloch functions closed to a critical point $\mathbf{k}_0$ of the Brillouin zone and $f_{i,n}(\mathbf{r})$ are slowly varying functions at the nanoscale, incorporating the information on the size and shape of the nanoparticle. It appears clearly that a proper account of the symmetry for $\psi_i(\mathbf{r})$ is not straightforward, provided that $u_{n,\mathbf{k}_0}(\mathbf{r})$ are related to double space group IRs of the 3D lattice, while $f_{i,n}(\mathbf{r})$ correspond to simple point group IRs of the nanostructure shape.

The proper symmetry-based treatment of this new type of tensorial product between a mesoscopic and atomistic quantities has been proposed only recently by M.A. Dupertuis and coworkers with the introduction of a general formalism of maximal symmetrization and reduction of fields [70, 71]. However for early computations of III–V nanostructure electronic wavefunctions [72], the shapes of the nanostructures were considered in many cases to be roughly compatible with the four-fold axes of the zinc-blende, avoiding elaborate symmetry-based procedures. In other cases involving nanostructure cylindrical shapes with the infinite axis parallel to one of the zinc-blende four-fold axes [73], it was shown that a few approximations on the bulk k.p Hamiltonian followed by a unitary transformation of the Bloch functions, allows a complete approach of the symmetry of $\psi_i(\mathbf{r})$, including strain, piezoelectric and non-linear piezoelectric effects [74]. A similar methodology can be used for inhomogeneous and strained wurtzite quantum nanostructures [75].

From that perspective, the first symmetry-based approach to $\psi_i(\mathbf{r})$ for a perovskite nanostructure was including a complex dependence of the bulk Bloch functions $u_{n,\mathbf{k}_0}(\mathbf{r})$ on the cubic, tetragonal or orthorhombic perovskite lattice structural instabilities, but assuming cubic nanostructure shapes for a simplified treatment [76]. This approach was quickly extended by various authors [77, 78]. Conversely, Nestoklon and coworkers were considering a reduction of symmetry due to the anisotropy cubic, tetragonal or orthorhombic nanostructure shapes, but relying on a basis of cubic bulk Bloch functions [79]. More detailed approaches to the computation of symmetry-based $\psi_i(\mathbf{r})$ have not yet been implemented for more realistic perovskite nanostructures, such as cuboids. To illustrate such a situation, let us consider a nanostructure with a tetragonal shape associated to a tetragonal distortion of the perovskite lattice. The simplest situation corresponds to the nanostructure four-fold axis being parallel to the tetragonal axis of the perovskite lattice, and a more complex case to the two axes perpendicular to each other. One may assume in this last case, that the incompatibility between the two axes directions simply results in some approximate descent of symmetry toward an orthorhombic symmetry. But, the proper methodology is more complex and requires to design an optimal basis related to combinations of Bloch functions as well as ultimately reduced envelope functions in this new basis [70].

3. Realistic electronic structure of metal halide frames in presence of SOC and optical response

After discussing the effect of dimensionality and point defects on the atomic orbital interaction in halide perovskite frames, we consider here a more realistic description of the electronic structure of these systems, by introducing the effect of SOC. As the most performant halide perovskites are based on heavy tin and lead metal, SOC turns out to be very important and therefore should not be regarded as simple perturbation of the electronic structure but should be explicitly accounted [42, 62]. Inclusion of SOC requires the introduction of double groups, which are deduced from the product of the $D_{1/2} = E_{1/2g}$ IR associated to the electron spin with the IR of the simple space group. Once this is done for the case of the cubic Pm-3m lattice metal halide perovskite, one obtains that the valence band edge is finally associated to R_6^+ IR, while the triply degenerated conduction band minimum, splits into two-fold R_6^- ($E_{1/2u}$) and four-fold R_8^- ($E_{3/2u}$) bands. These predictions are nicely confirmed by periodic DFT calculations in figure 5(a), performed on a cubic Pm-3m lattice of the CsPbI$_3$ perovskite [42, 58]. Indeed, explicit calculations clearly show a splitting of 1.62 eV for the conduction band edge at the R point of the first Brillouin zone.

Symmetry allows also to establish whether an optical transition is permitted or not. The rate for the probability of an optical transition from the initial state *i* to a final state *f* is given by the Fermi golden rule [59]:

$$\frac{dP_{i\to f}}{dt} \propto \left|\psi_f|\mathbf{r}|\psi_i\right|^2 \delta\left(E_c - E_v + \hbar\varpi\right) \tag{3}$$

where ψ_f and ψ_i are the corresponding wavefunctions, $\mathbf{r}$ is the perturbing dipole operator and the Dirac delta expresses the condition for energy conservation following the absorption of a photon with energy $\hbar\varpi$. Optical transitions are allowed if the inner product of the IR of the initial and final states $\chi_i \otimes \chi_f$ contains the IR of the dipole operator (corresponding to T_{1u} in the Pm-3m space group) [81]. In table 1, we report the symmetry analysis of the optical transition for the case of the Pm-3m AMX$_3$ perovskite lattice, starting from simple band-to-band picture of the optical absorption processes and progressively introducing the effect of excitonic interactions and SOC. Band-to-band transitions are related to the excitation of one electron from the valence to the conduction band-edge single particle states. Without SOC, the direct product of the IR of the valence and conduction band edges contains the IR of the perturbing dipole operator (T_{1u}) and the transition is therefore allowed, triply degenerate and isotropic. In the Wannier picture, the excitonic transition from ground state to the excited state is instead related to an additional Coulomb interaction term between electron and hole in the excited state. The IR of the lowest energy excited state hence corresponds to
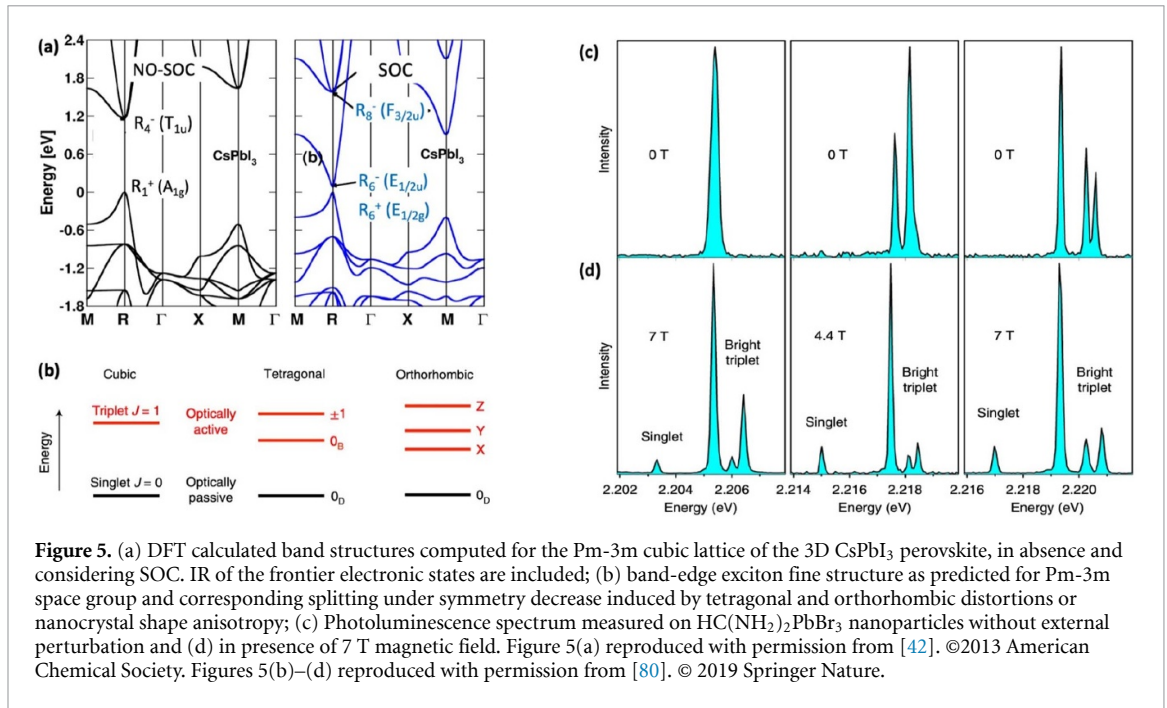
Figure 5. (a) DFT calculated band structures computed for the Pm-3m cubic lattice of the 3D CsPbI$_3$ perovskite, in absence and considering SOC. IR of the frontier electronic states are included; (b) band-edge exciton fine structure as predicted for Pm-3m space group and corresponding splitting under symmetry decrease induced by tetragonal and orthorhombic distortions or nanocrystal shape anisotropy; (c) Photoluminescence spectrum measured on HC(NH$_2$)$_2$PbBr$_3$ nanoparticles without external perturbation and (d) in presence of 7 T magnetic field. Figure 5(a) reproduced with permission from [42]. ©2013 American Chemical Society. Figures 5(b)–(d) reproduced with permission from [80]. © 2019 Springer Nature.

Table 1. Symmetry analysis for optical transitions in AMX$_3$ perovskites with cubic symmetry (Pm-3 m space group), represented as single particle band-to-band transitions and excitonic transitions. The analysis is performed both without and with SOC.

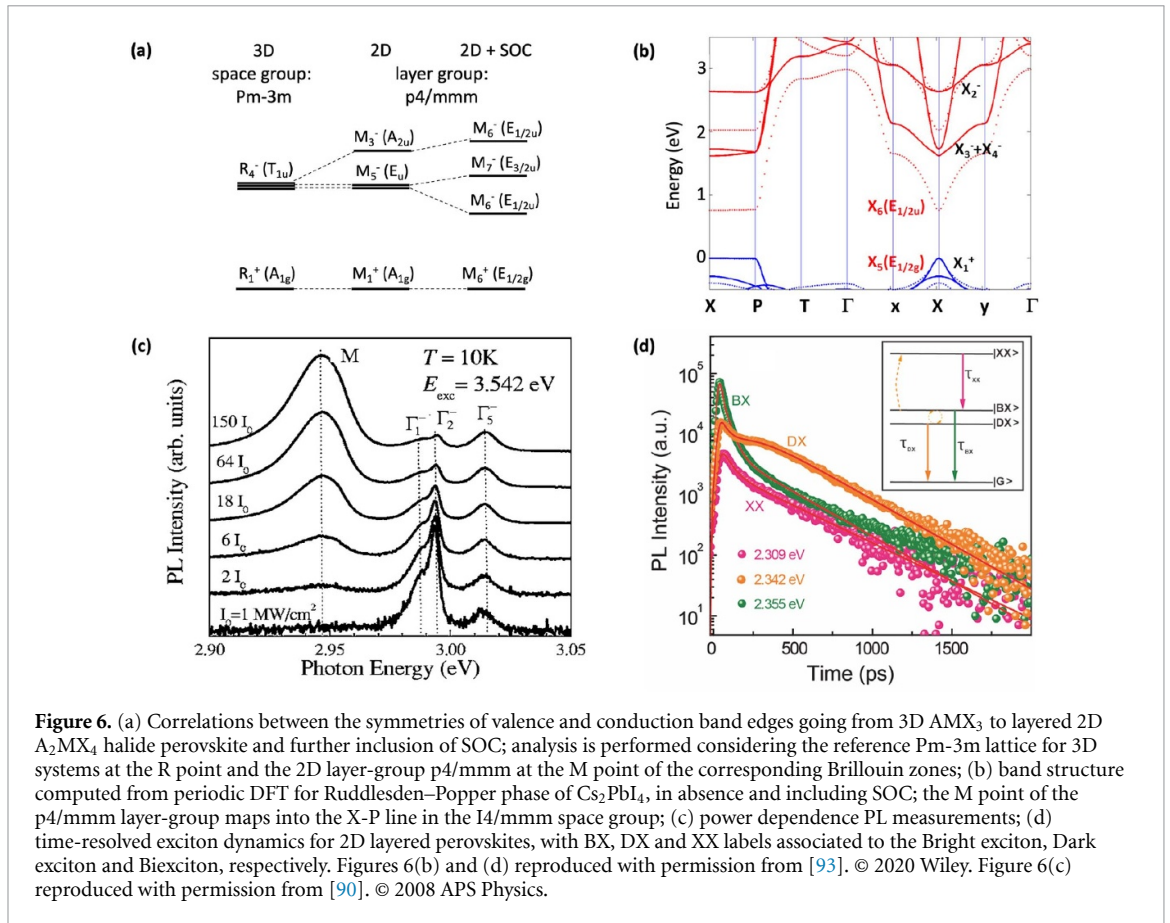| Band-to-band transition	Excitonic transition
ψ_i: valence band edge	ψ_i: ground state
ψ_f: conduction band edge	ψ_f: lowest energy excited state
	Without spin–orbit coupling
IR$(\psi_i) = R_1^+$ (A$_{1g}$)	IR$(\psi_i) = \Gamma_1^+$ (A$_{1g}$)
IR$(\psi_f) = R_4^-$ (T$_{1u}$)	IR$(\psi_f) = R_1^{+*} \otimes R_4^- \otimes \Gamma_1^+ = \Gamma_4^-$ (T$_{1u}$)
$\chi_i^* \otimes \chi_f = $ **T$_{1u}$ allowed**	$\chi_i^* \otimes \chi_f = $ **T$_{1u}$ allowed**
	With spin–orbit coupling
IR$(\psi_i) = R_6^+$ (E$_{1/2g}$)	IR$(\psi_i) = \Gamma_1^+$ (A$_{1g}$)
IR$(\psi_f) = R_6^-$ (E$_{1/2u}$)	IR$(\psi_f) = R_6^{+*} \otimes R_6^- \otimes \Gamma_1^+ = \Gamma_1^- + \Gamma_4^-$
	(A$_{1u}$ + T$_{1u}$)
$\chi_i^* \otimes \chi_f = $ A$_{1u}$ + **T$_{1u}$** forbidden + **allowed**	$\chi_i^* \otimes \chi_f = $ A$_{1u}$ + **T$_{1u}$** forbidden + **allowed**

the product of the IR of the valence and conduction band edges with a S-like envelope function (A$_{1g}$). Ultimately, for the lowest excited state of the Wannier progression the selection rules correspond to those of the single particle transitions but notice that this is not necessarily the case for higher components of the Wannier series, since the symmetry of the envelope function for the electron–hole correlated motion has to be included [54]. Inclusion of SOC brings to an important difference, as the lowest energy excited state corresponds in this case to an allowed triplet (triply degenerate) T$_{1u}$ transition, plus a forbidden singlet A$_u$ transition. This has not to be confused with the typical terminology used for organic semiconductors, where the triplet is indeed dark, while the singlet is bright [82]. The latter picture in fact relies on the separation of the radial and spin degrees of freedom, which is reasonable in Carbon-based semiconductors, while the results in table 1 are obtained by directly considering spinors and the total electron momentum. Hence, in the present case the terms 'singlet/triplet' are no more referred specifically to the pure-spin part of the wavefunction, but to a mixed space-spin description of the wavefunction.

In light of the small exciton binding energy reported for 3D lead-halide perovskite thin films and single crystals, on the order of 10 meV [83–85], excitonic effects are generally regarded as irrelevant in the photophysics of these semiconductors at room temperature. However, there is growing interest in understanding excitonic properties (fine structure, coupling with phonons, etc) for perovskite nanoparticles. These systems can be derived from the prototypical 3D perovskite structure, by reducing the corner-shared MX$_6$ octahedral connectivity down to few nanometers, corresponding to tens of AMX$_3$ consecutive chemical units [29]. Correspondingly, the spatial confinement of the electronic structure on the scale of the De-Broglie wavelength imparts unique features, like the enhancement electron–hole interaction, promising for light application [13, 14]. In this context, the observation of one, two or three lines in the optical emission

spectrum of $CsPbBr_3$ cubic-like nanocrystals, was initially attributed to possible underlying cubic, tetragonal and orthorhombic crystallographic structures (see figures 5(b) and (c)) [76]. In fact, the short- range exchange interaction between $E_{1/2u}$ (CB) and $E_{1/2g}$ (VB) monoelectronic edge states is expected to influence the Bloch function symmetries and lead to the exciton bright triplet splitting typical of respectively Oh, D4h and D2h exciton point symmetries. It is worth to note that in [76, 80], the theoretical analysis of the optical response of lead-bromine related nanoparticles is performed on the basis of the 3D cubic model (figure 2). This fact is in part justified by the fact that the continuum corner-shared octahedral connectivity, although limited to the nanometer scale, is expected to result in single particle states delocalized throughout all the nanoparticle, resembling Block waves in the parental 3D case. Another interpretation for the appearance of several lines in the optical spectrum of $CsPbBr_3$ nanoparticles is related to the effect of the perovskite nanocrystal shape anisotropy on the long-range part of the exchange interaction, influencing the Wannier exciton envelope function [79]. Further symmetry reductions were considered in another contribution [78], in which the high brightness of the emission was attributed to the unusual localization of the exciton dark state above the bright triplet due to a strong Rashba effect. However, the only direct observation of a perovskite nanocrystal dark state performed so far for $HC(NH_2)_2PbBr_3$ by using an external magnetic field, is yielding a more classical ordering, as shown in figure 5(c) [80]. In this work, the authors demonstrate that a dipole-forbidden exciton component is present in the low-energy part of the spectrum and gains optical intensity under the presence of an external magnetic field (see figure 5(d)). This funding nicely agrees with the $A_{1u} + T_{1u}$ fine-exciton structure predicted from the 3D case (table 1), with the external magnetic field mixing the optically forbidden A_{1u} component with the triply degenerate allowed T_{1u} components. The high brightness of the bright triplet emission was rather attributed to a second order phonon relaxation process. The dark-bright exciton splitting computed from the long-range exchange interaction was also in fair agreement with the experimental observations [80].

An isolated MX_6 octahedron represents another example of 0D nanostructure, where the spatial confinement results from the total interruption of the corner-shared connectivity of the MX_6 octahedra. An interesting technological case for lead-based systems corresponding to this situation is Cs_4PbBr_6, a system crystallizing in the space group R-3c and consisting in chemically unconnected octahedral separated by Cs cations [86]. This system has attracted considerable attention, due to reported photoluminescence quantum yield ranging between 40% and 45% [67, 68, 87], resulting from the enhancement of the electron–hole interaction, as due to the confinement of the electronic structure on the isolated Cs_4PbBr_6 octahedron. In this sense, the interruption of the octahedral connectivity seems to play a crucial role in determining the positive emission properties of this system, although alternative explanations have been proposed in the literature, as related to defects or emission from other phases [88]. As we aim here just to provide a symmetry perspective for a real case of lead-based system with isolated octahedral, we disregard about more complex questions and we focus on the electronic structure of R-3 c phase of Cs_4PbBr_6, as computed from DFT (see supporting information). Our calculations nicely agree with previous results from the literature [68, 87], showing that in absence of SOC the material is an indirect semiconductor but with direct transition in Γ which lies just few meV higher in energy. Focusing on the transition at Γ, our calculations predict valence and conduction band edges belonging to A_{2g} and A_{1u} IR, respectively, hence resulting in a dipole allowed transition of A_{2u} symmetry, both in the band-to-band and in the Wannier exciton frame (see table 1), consistently with the effective emission from these materials. Further inclusion of SOC, via the introduction of double group, results in exciton transition at Γ corresponding to $E_{1/2g} \otimes E_{1/2u} \otimes A_{1g} = A_{1u} + A_{2u} + E_u$. Group theory analysis hence predicts that the exciton fine structure of Cs_4PbBr_6 contains one dark state (A_{1u}) and three bright states, one polarized along the rhombohedral axis of C_3-symmetry (A_{2u}) and two degenerate components with in-plane polarization (E_u), similar to that of $CsPbBr_3$ nanoparticles undergoing towards tetragonal distortions. However, because of the enhanced electron–hole interaction for isolated $PbBr_6$ octahedra, it is reasonable to expect much larger splitting of the exciton fine structure for this case than for 3D nanoparticles. In this frame, spectroscopic measurements of the excitonic fine structure of Cs_4PbBr_6 could clarify the mechanism of light emission in this system.

We now focus on the role of SOC on the electronic structure and optical properties of bulk layered 2D perovskites. We showed before that the symmetry reduction from the 3D cubic space group to the layer-group already brings to the splitting of the triply degenerate conduction band edge into a two-fold state (M_5^-) and a non-degenerate state (M_3^-), as illustrated in figure 6(a). Further inclusion of SOC results in additional splitting of the former band, in two states with M_6^- and M_7^- symmetry. When considering interlayer stacking, in the specific case of the RP phase, one finds that the M point of the 2D first Brillouin zone of the p4/mmm layer-group maps into the X and P points of the 3D first Brillouin zone of the I4/mmm space group, with X and P differing in the electronic interaction between planes. DFT calculation for RP of Cs_2PbI_4 reported in figure 6(b) predict in fact a ~1.2 eV SOC-induced splitting of the conduction band at X point of the Brillouin zone, in X_2^- and $X_3^- + X_4^-$ IR. We may notice almost flat dispersions of the electronic

Figure 6. (a) Correlations between the symmetries of valence and conduction band edges going from 3D AMX_3 to layered 2D A_2MX_4 halide perovskite and further inclusion of SOC; analysis is performed considering the reference Pm-3m lattice for 3D systems at the R point and the 2D layer-group p4/mmm at the M point of the corresponding Brillouin zones; (b) band structure computed from periodic DFT for Ruddlesden–Popper phase of Cs_2PbI_4, in absence and including SOC; the M point of the p4/mmm layer-group maps into the X-P line in the I4/mmm space group; (c) power dependence PL measurements; (d) time-resolved exciton dynamics for 2D layered perovskites, with BX, DX and XX labels associated to the Bright exciton, Dark exciton and Biexciton, respectively. Figures 6(b) and (d) reproduced with permission from [93]. © 2020 Wiley. Figure 6(c) reproduced with permission from [90]. © 2008 APS Physics.

bands along the X $\rightarrow$ P direction, both in absence and when including SOC, that demonstrates the weakness of the electronic coupling between inorganic planes, because of the large inter-planar distance. The interlayer coupling is only revealed by a small splitting of the CB ($X^{3-} + X^{4-}$) in the absence of SOC and related to the centering of the unit cell for the I4/mmm conventional cell.

It is now well-known that spatial confinement of the frontier orbital in an atomically-thin layer and the dielectric contrast between the inorganic and the organic components enhance electron–hole interaction [34], resulting in exciton binding energy in the order of 450 meV [52]. As a result, excitons dominate the optoelectronic response of 2D layered perovskite. Thus, it is worth analyzing the symmetry of the lowest energy excitonic transition in order to determine its fine-structure. In this case, the IR of the exciton ground state, determined as in table 1 from the direct product of the IR of the valence ($E_{1/2g}$) and conduction ($E_{1/2u}$) band edges with a S-like envelope function (A_{1g}), results in $A_{1u} + A_{2u} + E_u$ IR for the exciton fine structure. This corresponds to the Γ_1^-, Γ_2^- and Γ_5^- assignment, often reported in the early literature, as illustrated in figure 6(c) [89–92]. Hence, as in the 3D case, the ground state exciton fine structure consists in a dark (A_{1u}) state and three bright states, two with in-plane polarization (E_u) and one with out-of-plane polarization (A_{2u}), in agreement with earlier theoretical predictions [63]. Further considering a symmetry reduction due to a monoclinic lattice distortion, as for the case of the actual crystallographic structure of the $(PEA)_2PbI_4$ (PEA = phenylethynyl-ammonium) RP phase, leads to a modified symmetry decomposition for the band-edge exciton fine structure in the C_{2h} IR: $2A_u + 2B_u$. This is essentially predicting that the expected purely dark state is mixed with the out-of-plane polarization singlet ($A_{1u} \rightarrow A_u$ and $A_{2u} \rightarrow A_u$), leading to two weakly observable emission lines close together in good agreement with recent experimental observation, which underlines the important role of the dark state on the photophysics of $(PEA)_2PbI_4$ [93]. For these systems an unusual bi-exciton dynamics was measured using time-dependent photoluminescence and it was hence proposed that a dark (or weakly allowed) excitonic state is involved in the bi-exciton emission, as schematized in figure 6(d).

We conclude this symmetry analysis focusing on the expected optical properties of d-HP. This class of perovskite systems has been only recently discovered and therefore its optical response has not been subjected to detailed experimental characterization, as in the case of 3D and 2D halide perovskites, yet [24, 25]. In this sense, symmetry arguments can already anticipate important differences with respect to the pristine 3D and layered 2D cases. Predictions from the previous Section are schematized in figure 7(a), nicely
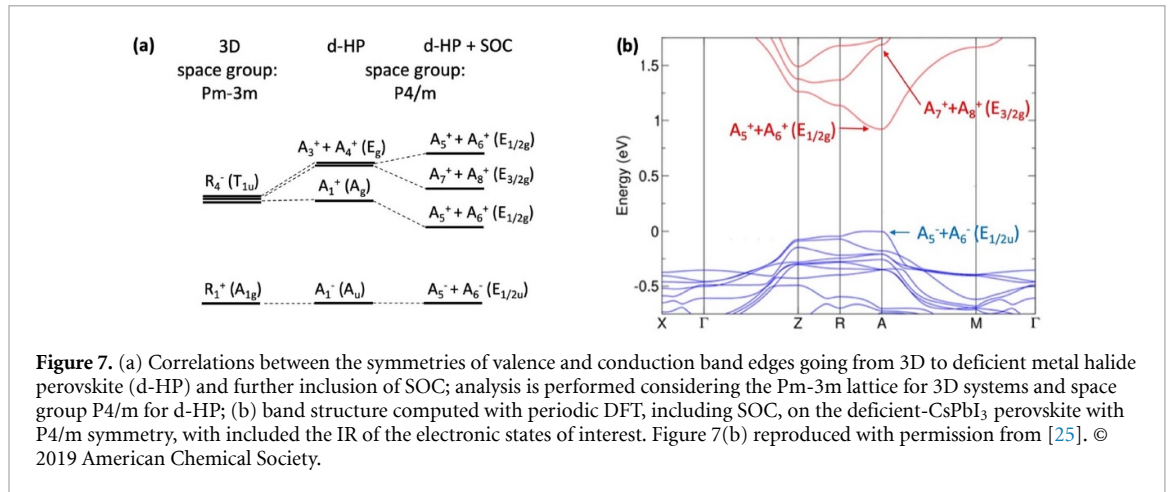
Figure 7. (a) Correlations between the symmetries of valence and conduction band edges going from 3D to deficient metal halide perovskite (d-HP) and further inclusion of SOC; analysis is performed considering the Pm-3m lattice for 3D systems and space group P4/m for d-HP; (b) band structure computed with periodic DFT, including SOC, on the deficient-CsPbI$_3$ perovskite with P4/m symmetry, with included the IR of the electronic states of interest. Figure 7(b) reproduced with permission from [25]. © 2019 American Chemical Society.

confirmed by the band structure from periodic DFT calculations in figure 7(b). In absence of SOC, DFT nicely confirms that the triply degenerate conduction band edge splits into doubly degenerate in-plane $A_3^+ + A_4^+$ state and non-degenerate out-of-plane A_1^+ state, with the latter being more stable. In addition, symmetry anticipates that SOC induces further splitting for the higher $A_3^+ + A_4^+$ component of the conduction band, as confirmed by DFT, (0.47 eV computed splitting). From these results, we can anticipate that the band-edge exciton fine structure of deficient perovskites only consists in optically bright states, in striking contrast to 3D and 2D structures, where one dark state was found. Indeed, the IR of the lowest energy excitonic state, as estimated from the inner product of the IR of the valence ($E_{1/2g}$) and conduction ($E_{1/2u}$) band edges with a S-like envelope function (A_g) results in $2A_u + E_u$ IR, where the first two components have out-of-plane polarization, while the latter doubly degenerate component has in-plane polarization. In other words, the decrease of symmetry, as due to the presence of the defect in the crystal lattice, results in a relaxation of the selection rules, with the dark A_{1u} state of the parental 3D compound acquiring optical intensity from the T_{1u} states of the pristine systems. Further experimental investigation of these systems under magnetic field, as done in [80], and performed on samples with controlled content of defects are recommended, in order to confirm the current prediction. In this sense, it would be interesting to investigate how the absence of optically dark excited state can affect the photophysics of deficient perovskites, considering the role of such states in the case of 3D perovskites [80], and 2D perovskites [93].

4. Conclusions

Detailed understanding of the photophysics of metal halide perovskites is a crucial step both for the full exploitation of these interesting semiconductors to fields where their potential has been widely assessed, namely photovoltaics and light emission, and also for their future usage for innovative applications, as lasing, sensing, spintronic, etc. In this frame, more and more involved experimental characterization studies of the optoelectronic response of halide perovskite materials have been reported in the recent literature, unveiling their excited state dynamics in the ultrafast regime, and/or under the effect of external fields [76, 78, 80, 84, 85, 93]. All these spectroscopic characterizations in turn greatly benefit from theoretical support and interpretation from symmetry analysis, traditionally used in the past to understand the properties of conventional inorganic semiconductors. Here, we provided a detailed symmetry analysis of halide perovskite structures of technological interest, namely the α-phase AMX$_3$ perovskites, as reference for nanoparticles, layered 2D perovskites and the recently introduced 'deficient' perovskites, as interesting study case to understand the effect of point defects in the crystalline structure of halide perovskitoids, down to isolated MX$_6$ octahedra, for the case of Cs$_4$PbBr$_6$ emitter. We highlighted how the change in symmetry, reflecting the change in dimensionality or the introduction of defects, modifies the electronic structure and optical response of metal halide perovskite materials. Meanwhile, we reviewed some of the recent results from the literature, as the current debate on the energetic order of the band-edge excitonic fine structure of perovskite nanoparticles [76, 78, 80]. Furthermore, we predict the exciton fine structure of pure R-3c Cs$_4$PbBr$_6$ crystals and d-HP structures, anticipating that these may show significant differences with respect to the 2D and 3D case, as due to confinement of the electronic state in one PbBr$_6$ octahedron (Cs$_4$PbBr$_6$) or due to the perturbation of the ideal lattice associated to point defects (d-HP). For d-HP in particular, we predict the presence of four bright excited states in the band-edge exciton fine structure, as result of the relaxation of symmetry rules due to the inclusion of point defect. We hope this work will become a useful reference to

frame symmetry properties of metal halide perovskite in a broad context and will inspire similar analyses and additional spectroscopic measurement for these and other cases of technological interest.

Acknowledgments

ORCID iD

Claudio Quarti ⬤ https://orcid.org/0000-0002-5488-1216

References

[1] Kojima A, Teshima K, Shirai Y and Miyasaka T 2009 Organometal Halide Perovskites as Visible-Light Sensitizers for Photovoltaic Cells *J. Am. Chem. Soc.* **131** 6050–1

[2] Lee M M, Teuscher J, Miyasaka T, Murakami T N and Snaith H J 2012 Efficient hybrid solar cells based on meso-superstructured organometal halide perovskites *Science* **338** 643–7

[3] Liu M, Johnston M B and Snaith H J 2013 Efficient planar heterojunction perovskite solar cells by vapour deposition *Nature* **501** 395–8

[4] Heo J H *et al* 2013 Efficient inorganic–organic hybrid heterojunction solar cells containing perovskite compound and polymeric hole conductors *Nat. Photonics* **7** 486–91

[5] Zhou H, Chen Q, Li G, Luo S, Song T, Duan H-S, Hong Z, You J, Liu Y and Yang Y 2014 Interface engineering of highly efficient perovskite solar cells *Science* **345** 542–6

[6] Jeon N J, Noh J H, Yang W S, Kim Y C, Ryu S, Seo J and Seok S I 2015 Compositional engineering of perovskite materials for high-performance solar cells *Nature* **517** 476–80

[7] Grancini G *et al* 2017 One-year stable perovskite solar cells by 2D/3D interface engineering *Nat. Commun.* **8** 15684

[8] Jeon N J, Na H, Jung E H, Yang T, Lee Y G, Kim G, Shin H-W, Seok S I, Lee J and Seo J 2018 A fluorene-terminated hole-transporting material for highly efficient and stable perovskite solar cells *Nat. Energy* **3** 682–9

[9] www.nrel.gov/pv/cell-efficiency.html

[10] www.nrel.gov/pv/module-efficiency.html

[11] Tan Z-K *et al* 2014 Bright light-emitting diodes based on organometal halide perovskite *Nat. Nanotechnol.* **9** 687–92

[12] Yuan M *et al* 2016 Perovskite energy funnels for efficient light-emitting diodes *Nat. Nanotechnol.* **11** 872–7

[13] Lin K *et al* 2018 Perovskite light-emitting diodes with external quantum efficiency exceeding 20 per cent *Nature* **562** 245–8

[14] Xu W *et al* 2019 Rational molecular passivation for high-performance perovskite light-emitting diodes *Nat. Photonics* **13** 418–24

[15] De Wolf S, Holovsky J, Moon S-J, Löper P, Nielsen B, Ledinsky M, Haug F-J, Yum J-H and Ballif C 2014 Organometallic halide perovskites: sharp optical absorption edge and its relation to photovoltaic performance *J. Phys. Chem. Lett.* **5** 1035–9

[16] Meggiolaro D, Motti S G, Mosconi E, Barker Alex J, Ball J, Perini C A R, Deschler F, Petrozza A and De Angelis F 2018 Iodine chemistry determines the defect tolerance of lead-halide perovskites *Energy Environ. Sci.* **11** 702–13

[17] Kang J and Wang L-W 2017 High defect tolerance in lead halide perovskite CsPbBr$_3$ *J. Phys. Chem. Lett.* **8** 489–93

[18] Wehrenfennig C, Eperon G E, Johnston M B, Snaith H J and Herz L 2014 Charge carrier mobilities and life- times in organolead trihalide perovskites *Adv. Mater.* **26** 1584–9

[19] Stranks S D, Eperon G E, Grancini G, Menelaou C, Alcocer M J P, Leijtens T, Herz L, Petrozza A and Snaith H J 2013 Electron-Hole diffusion lengths exceeding 1 micrometer in an organometal trihalide perovskite absorber *Science* **342** 341–4

[20] Xing G, Mathews N, Sun S, Lim S S, Lam Y M, Grätzel M, Mhaisalkar S and Sum T C 2013 Long-range balanced electron-and hole-transport lengths in organic–inorganic CH$_3$NH$_3$PbI$_3$ *Science* **342** 344–7

[21] Ke W *et al* 2017 Enhanced photovoltaic performance and stability with a new type of hollow 3D perovskite enFASnI3 *Sci. Adv* **3** e1701293

[22] Tsai C-M, Lin Y-P, Pola M K, Narra S, Jokar E, Wang Y-W and Diau E W-G 2018 Control of crystal structures and optical properties with hybrid formamidinium and 2-hydroxyethylammonium cations for mesoscopic carbon-electrode tin-based perovskite solar cells *ACS Energy Lett.* **3** 2077–85

[23] Spanopoulos I, Ke W, Stoumpos C C, Schuelle E C, Kontsevoi Oleg Y, Seshadri R and Kanatzidis M G 2018 Unraveling the chemical nature of the 3D "hollow" hybrid halide perovskites *J. Am. Chem. Soc.* **140** 5728–42

[24] Leblanc A, Mercier N, Allain M, Dittmer J, Fernandez V and Pauporté T 2017 Lead- and iodide-deficient (CH$_3$NH$_3$)PbI$_3$ (d-MAPI): the bridge between 2D and 3D hybrid perovskites *Angew. Chem. Int. Ed.* **56** 16067–72

[25] Leblanc A, Mercier N, Allain M, Dittmer J, Pauporté T, Fernandez V, Boucher F, Kepenekian M and Katan C 2019 Enhanced stability and band gap tuning of α-[HC(NH$_2$)$_2$]PbI$_3$ hybrid perovskite by large cation integration *ACS Appl. Mater. Interfaces* **11** 20743–51

[26] Grancini G and Nazeeruddin M K 2019 Dimensional tailoring of hybrid perovskites for photovoltaics *Nat. Rev. Mater.* **4** 4–22

[27] Saidaminov M I, Mohammed O F and Bakr O M 2017 Low-dimensional-networked metal halide perovskites: the next big thing *ACS Energy Lett.* **2** 889–96

[28] Huang X, Guo Q, Yang D, Xiao X, Liu X, Xia Z, Fan F, Qiu J and Dong G 2020 Reversible 3D laser printing of perovskite quantum dots inside a transparent medium *Nat. Photon.* **14** 82–88

[29] Zheng K, Zhu Q, Abdellah M, Messing M A, Zhang W, Generalov A, Niu Y, Ribaud L, Canton S E and Pullerits T 2015 Exciton binding energy and the nature of emissive states in organometal halide perovskites *J. Phys. Chem. Lett.* **6** 2969–75

[30] Zhao Q *et al* 2019 High efficiency perovskite quantum dot solar cells with charge separating heterostructure *Nat. Commun.* **10** 2842

[31] Hao M *et al* 2020 Ligand-assisted cation-exchange engineering for high-efficiency colloidal $Cs_{1-x}FA_xPbI_3$ quantum dot solar cells with reduced phase segregation *Nat. Energy* **5** 79–88

[32] Mitzi D B, Feild C A, Harrison W T A and Guloy A M 1994 Conducting tin halides with a layered organic-based perovskite structure *Nature* **369** 467–9

[33] Smith M D, Connor B A and Karunadasa H I 2019 Tuning the luminescence of layered halide perovskites *Chem. Rev.* **119** 3104–39

[34] Katan C, Mercier N and Even J 2019 Quantum and dielectric confinement effects in lower-dimensional hybrid perovskite semiconductors *Chem. Rev.* **119** 3140–92

[35] Dou L *et al* 2015 Atomically thin two-dimensional organic-inorganic hybrid perovskites *Science* **349** 1518–21

[36] Tsai H *et al* 2018 Stable light-emitting diodes using phase-pure Ruddlesden–Popper layered perovskites *Adv. Mater.* **30** 1704217

[37] Tsai H *et al* 2016 High-efficiency two-dimensional Ruddlesden–popper perovskite solar cells *Nature* **536** 312–6

[38] Zheng C, Rubel O, Kepenekian M, Rocquefelte X and Katan C 2019 Electronic properties of Pb-I deficient lead halide perovskites *J. Chem. Phys.* **151** 234704

[39] Marronnier A, Lee H, Geffroy B, Even J, Bonnassieux Y and Roma G 2017 Structural instabilities related to highly anharmonic phonons in halide perovskites *J. Phys. Chem. Lett.* **8** 2659–65

[40] Carignano M, Assa Aravind S, Roqan I S, Even J and Katan C 2017 Critical fluctuations and anharmonicity in lead iodide perovskites from molecular dynamics supercell simulations *J. Phys. Chem. C* **121** 20729–38

[41] Quarti C, Mosconi E, Ball J, D'Innocenzo V, Tao C, Pathak S, Snaith H J, Petrozza A and De Angelis F 2016 Structural and optical properties of methylammonium lead iodide across the tetragonal to cubic phase transition: implications for perovskite solar cells *Energy Environ. Sci.* **9** 155–63

[42] Even J, Pedesseau L, Jancu J-M and Katan C 2013 Importance of spin–orbit coupling in hybrid organic/inorganic perovskites for photovoltaic applications *J. Phys. Chem. Lett.* **4** 2999–3005

[43] Umari P, Mosconi E and De Angelis F 2015 Relativistic GW calculations on $CH_3NH_3PbI_3$ and $CH_3NH_3SnI_3$ perovskites for solar cell applications *Sci. Rep.* **4** 4467

[44] Brivio F, Butler K T, Walsh A and van Schilfgaarde M 2014 Relativistic quasiparticle self-consistent electronic structure of hybrid halide perovskite photovoltaic absorbers **89** 155204

[45] Umari P, Mosconi E and De Angelis F 2018 Infrared dielectric screening determines the low exciton binding energy of metal-halide perovskites *J. Phys. Chem. Lett.* **9** 620–7

[46] Mattoni A, Filippetti A, Saba M I and Delugas P 2015 Methylammonium rotational dynamics in lead halide perovskite by classical molecular dynamics: the role of temperature *J. Phys. Chem. C* **119** 17421–8

[47] Lahnsteiner J, Jinnouchi R and Bokdam M 2019 Long-range order imposed by short-range interactions in methylammonium lead iodide: comparing point-dipole models to machine-learning force fields *Phys. Rev. B* **100** 094106

[48] Poncé S, Schlipf M and Giustino F 2019 Origin of low carrier mobilities in halide perovskites *ACS Energy Lett.* **4** 456–63

[49] Hedley G J, Quarti C, Harwell J, Prezhdo O V, Beljonne D and Samuel I D W 2018 Hot-hole cooling controls the initial ultrafast relaxation in methylammonium lead iodide perovskite *Sci. Rep.* **8** 8115

[50] Thouin F, Valverde-Chavéz D A, Quarti C, Cortecchia D, Bargigia I, Beljonne D, Petrozza A, Silva C and Kandada A R S 2019 Phonon coherences reveal the polaronic character of excitons in two-dimensional lead halide perovskites *Nat. Mater.* **18** 349–56

[51] Even J, Pedesseau L, Jancu J-M and Katan C 2014 DFT and k · p modelling of the phase transitions of lead and tin halide perovskites for photovoltaic cells *Phys. Status Solidi RRL* **8** 31

[52] Blancon J-C *et al* 2018 Scaling law for excitons in 2D perovskite quantum wells *Nat. Commun.* **9** 2254

[53] Boyer-Richard S, Katan C, Traoré B, Scholz R, Jancu J-M and Even J 2016 Symmetry-based tight binding modeling of halide perovskite semiconductors *J. Phys. Chem. Lett.* **7** 3833–40

[54] Even J 2015 Pedestrian guide to symmetry properties of the reference cubic structure of 3D all-inorganic and hybrid perovskites *J. Phys. Chem. Lett.* **6** 2238–42

[55] Even J, Pedesseau L, Sapori D, Rolland A, Kepenekian M and Katan C 2016 Electronic properties of metal halide perovskites *Unconventional Thin Film Photovoltaics* (Cambridge: Royal Society of Chemistry) pp 202–33

[56] Ben Aich R, Ben Radhia S, Boujdaria K, Chamarro M and Testelin C 2020 Multiband k.p model for tetragonal crystals: application to hybrid halide perovskite nanocrystals *J. Phys. Chem. Lett.* **11** 808–18

[57] Poglitsch A and Weber D 1987 Dynamic disorder in methylammoniumtrihalogenoplumbates (II) observed by millimeter-wave spectroscopy *J. Chem. Phys.* **87** 6373–8

[58] Marronnier A, Roma G, Boyer-Richard S, Pedesseau L, Jancu J-M, Bonnassieux Y, Katan C, Stoumpos C C, Kanatzidis M G and Even J 2018 Anharmonicity and disorder in the black phases of cesium lead iodide used for stable inorganic perovskite solar cells *ACS Nano* **12** 3477–86

[59] Yu P Y and Cardona M 2005 *Fundamentals of Semiconductors* (Berlin: Springer)

[60] Bloch F 1929 Über die Quantenmechanik der Elektronen in Kristallgittern *Z. Phys.* **52** 555–600

[61] Umebayashi T, Asai K, Kondo T and Nakao A 2003 Electronic structures of lead iodide based low-dimensional crystals *Phys. Rev. B* **67** 155405

[62] Katan C, Pedesseau L, Kepenekian M, Rolland A and Even J 2015 Interplay of spin–orbit coupling and lattice distortion in metal substituted 3D tri-chloride hybrid perovskites *J. Mater. Chem. A* **3** 9232–40

[63] Even J, Pedesseau L, Dupertuis M-A, Jancu J-M and Katan C 2012 Electronic model for self-assembled hybrid organic/perovskite semiconductors: reverse band edge electronic states ordering and spin-orbit coupling *Phys. Rev. B* **86** 205301

[64] Schaak R E and Mallouk T E 2002 *Chem. Mater.* **14** 1455–71

[65] Maughan A E, Ganose A X, Scanlon D O and Neilson J R 2019 Perspectives and design principles of vacancy-ordered double perovskite halide semiconductors *Chem. Mater.* **31** 1184–95

[66] Dalpian G M, Liu Q, Stoumpos C C, Douvalis A P, Balasubramanian M, Kanatzidis M G and Zunger A 2017 Changes in charge density vs changes in formal oxidation states: the case of Sn halide perovskites and their ordered vacancy analogues *Phys. Rev. Mater.* **1** 025401

[67] Saidaminov M I, Almutlaq J, Sarmah S, Dursun I, Zhumekenov A, Begum R, Pan J, Cho N, Mohammed O F and Bakr O M 2016 Pure Cs_4PbBr_6: highly luminescent zero-dimensional perovskite solids *ACS Energy Lett.* **1** 840–5

[68] Almutlaq J, Yin J, Mohammed O F and Bakr O M 2018 The benefit and challenges of zero-dimensional perovskites *J. Phys. Chem. Lett.* **9** 4131–8

[69] Robert C *et al* 2016 Electronic wave functions and optical transitions in (In,Ga)As/GaP quantum dots *Phys. Rev. B* **94** 075445

[70] Dalessi S and Dupertuis M-A 2010 Maximal symmetrization and reduction of fields: application to wave functions in solid-state nanostructures *Phys. Rev. B* **81** 125106

[71] Svendsen G K, Skaar J, Weman H and Dupertuis M-A 2015 Symmetries and optical transitions of hexagonal quantum dots in GaAs/AlGaAs nanowires *Phys. Rev.* B **92** 205303

[72] Grundmann M, Stier O and Bimberg D 1995 InAs/GaAs pyramidal quantum dots: strain distribution, optical phonons, and electronic structure *Phys. Rev.* B **52** 11969

[73] Tadic M, Peeters F M and Janssens J 2002 Effect of isotropic versus anisotropic elasticity on the electronic structure of cylindrical InP/In0.49Ga0.51P self-assembled quantum dots *Phys. Rev.* B **65** 165333

[74] Even J, Doré F, Cornet C and Pedesseau L 2008 Semianalytical model for simulation of electronic properties of narrow-gap strained semiconductor quantum nanostructures *Phys. Rev.* B **77** 085305

[75] Even J 2009 Symmetry analysis and exact model for the elastic, piezoelectric, and electronic properties of inhomogeneous and strained wurtzite quantum nanostructures *Appl. Phys. Lett.* **94** 102105

[76] Fu M, Tamarat P, Huang H, Even J and Lounis B 2017 Neutral and charged exciton fine structure in single lead halide perovskite nanocrystals revealed by magneto-optical spectroscopy *Nano Lett.* **17** 2895–901

[77] Ramade J *et al* 2018 Fine structure of excitons and electron–hole exchange energy in polymorphic CsPbBr$_3$ single nanocrystals *Nanoscale* **10** 6393–401

[78] Becker M A *et al* 2018 Bright triplet excitons in caesium lead halide perovskites *Nature* **553** 189–93

[79] Nestoklon M O *et al* 2018 Optical orientation and alignment of excitons in ensembles of inorganic perovskite nanocrystal *Phys. Rev.* B **97** 235304

[80] Tamarat P, Bodnarchuk M I, Trebbia J-B, Rolf E, Kovalenko M V, Even J and Lounis B 2019 The ground exciton state of formamidinium lead bromide perovskite nanocrystals is a singlet dark state *Nat. Mater.* **18** 717–24

[81] Klingshirn C F 2012 *Semiconductor Optics* (Berlin: Springer)

[82] Pope M and Swenberg C E 1999 *Electronic Processes in Organic Crystals and Polymers* (Oxford : Oxford University Press)

[83] Fang -H-H, Wang F, Adjokatse S, Zhao N, Even J and Loi M A 2016 Photoexcitation dynamics in solution-processed formamidinium lead iodide perovskite thin films for solar cell applications *Light Sci. Appl.* **5** E16056

[84] Miyata A, Mitioglu A, Plochocka P, Portugall O, Wang J T-W, Stranks S D, Snaith H J and Nicholas R J 2015 Direct measurement of the exciton binding energy and effective masses for charge carriers in an organic–inorganic tri-halide perovskite *Nat. Phys.* **11** 582–7

[85] Baranowski M and Plochocka P 2020 Excitons in metal-halide perovskites *Adv. Energy Mater.* **10** 1903659

[86] Andrews R H, Clark S J and Donaldson J D 1983 Solid-state properties of materials of the type Cs$_4$MXs(where M = Sn or Pb and X = CI or Br) *J. Chem. Soc. Dalton Trans.* **10** 1903659

[87] Chen D, Wan Z, Chen X, Yuan Y and Zhong J 2016 Large-scale room-temperature synthesis and optical properties of perovskite-related Cs$_4$PbBr$_6$ fluorophores *J. Chem. Mater.* C **4** 10646

[88] Wang L, Liu H, Zhang Y and Mohammed O F 2020 Photoluminescence origin of zero-dimensional Cs$_4$PbBr$_6$ perovskite *ACS Energy Lett.* **5** 87–99

[89] Tanaka K, Takahashi T, Kondo T, Umeda K, Ema K, Umebayashi T, Asai K, Uchida K and Miura N 2005 Electronic and excitonic structures of inorganic–organic perovskite-type quantum-well crystal (C$_4$H$_9$NH$_3$)$_2$PbBr$_4$ *Jpn. J. Appl. Phys.* **44** 5923–32

[90] Ema K, Umeda K, Toda K, Yajima C, Arai Y and Kunugita H 2006 Huge exchange energy and fine structure of excitons in an organic–inorganic quantum well material *Phys. Rev.* B **73** 241310

[91] Ema K, Inomata M, Kato Y, Kunugita H and Era K 2008 Nearly perfect triplet-triplet energy transfer from Wannier excitons to naphthalene in organic-inorganic hybrid quantum-well materials *Phys. Rev. Lett.* **100** 257401

[92] Takagi H, Kunugita H and Ema K 2013 Influence of the image charge effect on excitonic energy structure in organic-inorganic multiple quantum well crystals *Phys. Rev.* B **87** 125421

[93] Fang -H-H, Yang J, Adjokatse S, Tekelenburg E, Kamminga M E, Duim H, Ye J, Blake G R, Even J and Loi M A 2020 Band-edge exciton fine structure and exciton recombination dynamics in single crystals of layered hybrid perovskites *Adv. Funct. Mater.* **30** 1907979